Dietary phytochemicals regulate whole-body CYP1A1 expression through an arylhydrocarbon receptor nuclear translocator–dependent system in gut

Shinji Ito, Chi Chen, Junko Satoh, SunHee Yim, and Frank J. Gonzalez

Laboratory of Metabolism, Center for Cancer Research, National Cancer Institute, Bethesda, Maryland, USA.

Cytochrome P450 1A1 (CYP1A1) is one of the most important detoxification enzymes due to its broad substrate specificity and wide distribution throughout the body. On the other hand, CYP1A1 can also produce highly carcinogenic intermediate metabolites through oxidation of polycyclic aromatic hydrocarbons. We describe what we believe to be a novel regulatory system for whole-body CYP1A1 expression by a factor originating in the gut. A mutant mouse was generated in which the arylhydrocarbon receptor nuclear translocator (Arnt) gene is disrupted predominantly in the gut epithelium. Surprisingly, CYP1A1 mRNA expression and enzymatic activities were markedly elevated in almost all non-gut tissues in this mouse line. The induction was even observed in early-stage embryos in pregnant mutant females. Interestingly, the upregulation was CYP1A1 selective and lost upon administration of a synthetic purified diet. Moreover, the increase was recovered by addition of the natural phytochemical indole-3-carbinol to the purified diet. These results suggest that an Arnt-dependent pathway in gut has an important role in regulation of the metabolism of dietary CYP1A1 inducers and whole-body CYP1A1 expression. This machinery might be involved in naturally occurring carcinogenic processes and/or other numerous biological responses mediated by CYP1A1 activity.

Introduction

In addition to its role in nutrient absorption, the intestine is also important for the metabolism of dietary toxins and orally absorbed drugs due to its extremely large surface area with complicated villous structure and its extensive xenobiotic metabolism and transport system (1–4). A number of xenobiotics such as the polycyclic aromatic hydrocarbons (PAHs) are known to bind and activate the basic helix-loop-helix/Per-Arnt-Sim (bHLH/PAS) transcription factor arylhydrocarbon receptor (AhR). AhR forms a heterodimer with the AhR nuclear translocator (Arnt). The AhR/Arnt heterodimer then activates target gene expression through binding to upstream xenobiotic response elements (XREs). AhR target genes are usually associated with chemical detoxification and include xenobiotic-metabolizing cytochromes P450 (5, 6). The AhR gene battery participates in regulating the metabolism of many xenobiotics in the intestine (4, 7, 8).

Cytochrome P450 1A1 (CYP1A1) is one of the most well-characterized xenobiotic-metabolizing enzymes regulated by the AhR. CYP1A1 is expressed in various tissues, including the small intestine (4, 8). PAHs are typical CYP1A1 substrates, while several atypical substrates, such as eicosanoids and plant indole derivatives, are also metabolized by this enzyme (9, 10). It was demonstrated that detoxification by CYP1A1 is important for protection from various deleterious effects of PAHs; paradoxically, however, CYP1A1 is also important for the metabolic activation of PAHs such as benzo[*a*]pyrene (BaP), a procarcinogen found in combustibles including tobacco smoke. These PAHs are converted to highly reactive electrophilic metabolites that can form DNA adducts and lead to gene mutations and cellular transformation (9).

Arnt, as the partner of AhR, is also called Hif-1β (hypoxia inducible factor–1β), a designation derived from another dimerization partner, Hif-1α (hypoxia inducible factor–1α). Hif-1α is degraded rapidly under normal oxygen pressure but stabilized under hypoxia to form a heterodimer with Arnt. The Hif-1α/β heterodimer, named Hif-1, activates expression of its target genes through hypoxia response elements (HREs) in response to low cellular oxygen supplies (11, 12). Thus, Arnt plays critical roles in at least 2 important biological responses to exogenous challenge.

To investigate the function of Arnt in the intestine, a mouse line containing a mutant *Arnt* allele (*Arnt flΔneo*), in which an essential exon is flanked by *loxP* sequences, was produced (13). This mouse line was then bred with a transgenic mouse line containing Cre recombinase that is controlled by the *villin* gene promoter (14, 15). Since *villin* is predominantly expressed in the epithelial cells of intestinal villi, the villin-Cre mouse expresses Cre recombinase almost exclusively in the intestinal epithelium. The *villin* gene is also expressed in the kidney cortex (16); however, in the villin-Cre mice, the protein expression and the recombination activity of Cre recombinase were significantly lower in kidney compared with intestinal epithelium (15). By crossing *Arnt flΔneo* homozygous mice ($Arnt^{F/F}$) with villin-Cre mice, a novel mutant mouse line ($Arnt^{\Delta IE}$) devoid of Arnt expression in the intestinal epithelium was generated.

Nonstandard abbreviations used: AhR, arylhydrocarbon receptor; Arnt, AhR nuclear translocator; BaP, benzo[*a*]pyrene; CYP1A1, cytochrome P450 1A1; Hif-1α, hypoxia inducible factor–1α; I3C, indole-3-carbinol; LC-MS, liquid chromatography–mass spectrometry; MS/MS, tandem mass spectrometry; *Mt1*, metallothionein 1; PAH, polycyclic aromatic hydrocarbon; PhIP, 2-amino-1-methyl-6-phenylimidazo[4,5-*b*]pyridine; PLS-DA, partial least-squares discriminant analysis; qPCR, quantitative RT-PCR; TOFMS, time-of-flight mass spectrometer; UPLC, ultra-performance liquid chromatography.

Conflict of interest: The authors have declared that no conflict of interest exists.

Citation for this article: *J. Clin. Invest.* **117**:1940–1950 (2007). doi:10.1172/JCI31647.

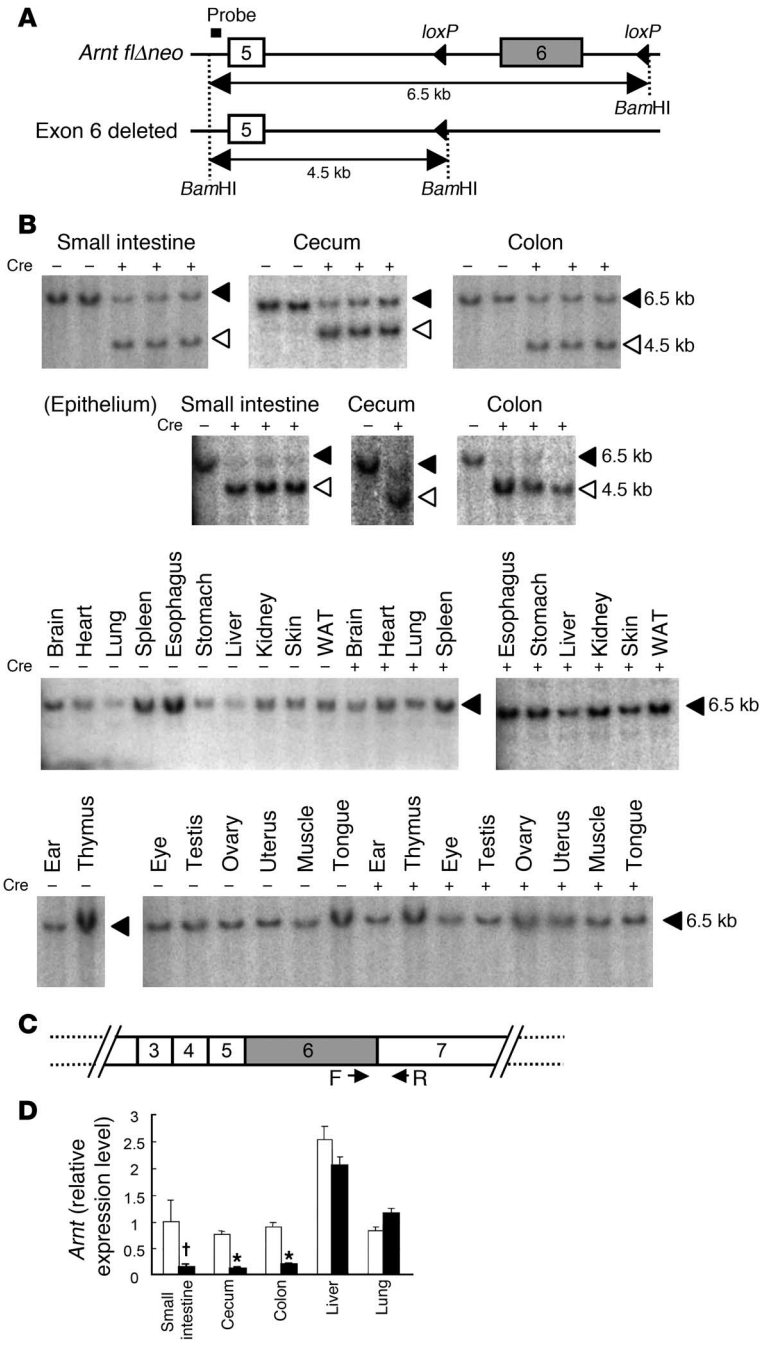

Figure 1
Intestinal epithelium–specific disruption of the *Arnt* gene. (**A**) Schematic structure of modified *Arnt* allele used in this study. The probe used for Southern blot analysis is indicated. (**B**) Southern blot analysis for the detection of the disrupted *Arnt* allele. Signals corresponding to the *Arnt flΔneo* allele and exon 6–deleted allele (13) are indicated by filled and open triangles, respectively. Cre^+ or Cre^- indicates the existence or absence of the Cre recombinase in the genome. WAT, white adipose tissue. (**C**) Primers used for detection of intact *Arnt* transcripts. (**D**) Relative expression levels of intact *Arnt* transcripts in the intestine, liver, and lung examined by qPCR. White and black bars represent the expression levels in $Arnt^{F/F}$ and $Arnt^{\Delta IE}$ mice, respectively. Average values for each group ($n = 4$) are shown. Relative values were calculated from the average expression level in the small intestine of the $Arnt^{F/F}$ mice with FVB/N background defined as general standard (1.0). Error bars indicate SEM. Statistical significance between the average values for $Arnt^{F/F}$ and $Arnt^{\Delta IE}$ mice in the same tissue was examined. $^*P < 0.05$; $^\dagger P < 0.05$.

Results

Intestinal epithelium–specific knockout of Arnt and Hif-1α genes. In order to determine the genomic DNA recombination efficiency in $Arnt^{\Delta IE}$ mice, the *Arnt* gene structure was examined by Southern blot analysis (Figure 1, A and B). As shown in Figure 1B, 2 fragments of different sizes were detected in the small intestine, cecum, and colon of $Arnt^{\Delta IE}$ mice; the upper band corresponds to the floxed allele, and the lower band corresponds to the exon 6–deleted allele (13). The upper band of $Arnt^{\Delta IE}$ mice was markedly diminished as compared with that of control mice when genomic DNA from the intestinal epithelium was examined (Figure 1B). In clear contrast, all non-gut tissues yielded only the upper band corresponding to the floxed *Arnt* allele (Figure 1B). These results indicated that genomic recombination at the floxed allele occurred only in the epithelial layer cells of the intestinal tract.

The expression levels of the functional *Arnt* transcripts were also examined by quantitative RT-PCR (qPCR) analysis using primers that amplify the exon 6–containing region (Figure 1C). As expected, expression of the intact Arnt mRNA was greatly decreased in the small intestine, cecum, and colon of $Arnt^{\Delta IE}$ mice, although faint, residual expression of this gene was still detectable. On the other hand, the Arnt mRNA levels were unchanged in non-gut tissues (Figure 1D).

A detailed analysis of the gene expression pattern of this intestine-specific *Arnt*-knockout mouse line revealed that the intestinal Arnt/AhR pathway could specifically suppress whole-body CYP1A1 expression with the involvement of dietary phytochemicals. This concept regarding the regulatory mechanism of xenobiotic metabolism was further validated by a proof-of-concept experiment, in which indole-3-carbinol (I3C), a natural CYP1A1 inducer, was administered through dietary supplementation (17). Since the plant-derived foods, which are rich in phytochemicals, are ubiquitous in the diet, this pathway should be of great importance for a wide variety of biological responses under the influence of CYP1A1 activities.

To discriminate the influences of the Hif-1α–dependent pathway from those of other pathways governed by Arnt, Hif-$1\alpha^{\Delta IE}$ mice lacking Hif-1α expression predominantly in the intestinal epithelium were also generated. This was achieved by the same strategies as those used to generate the $Arnt^{\Delta IE}$ mice: Hif-$1\alpha^{F/F}$ mice (18) were crossed with villin-Cre mice (15). DNA recombination at the Hif-1α locus and the elimination of intact Hif-1α mRNA expression in the gut epithelium were confirmed by the Southern blotting (Figure 2, A and B) and qPCR analyses using deleted exon–specific primers (Figure 2, C and D).

Gene expression profiles in the intestinal tract of $Arnt^{\Delta IE}$ mice. $Arnt^{\Delta IE}$ mice exhibited no apparent deleterious phenotype under normal

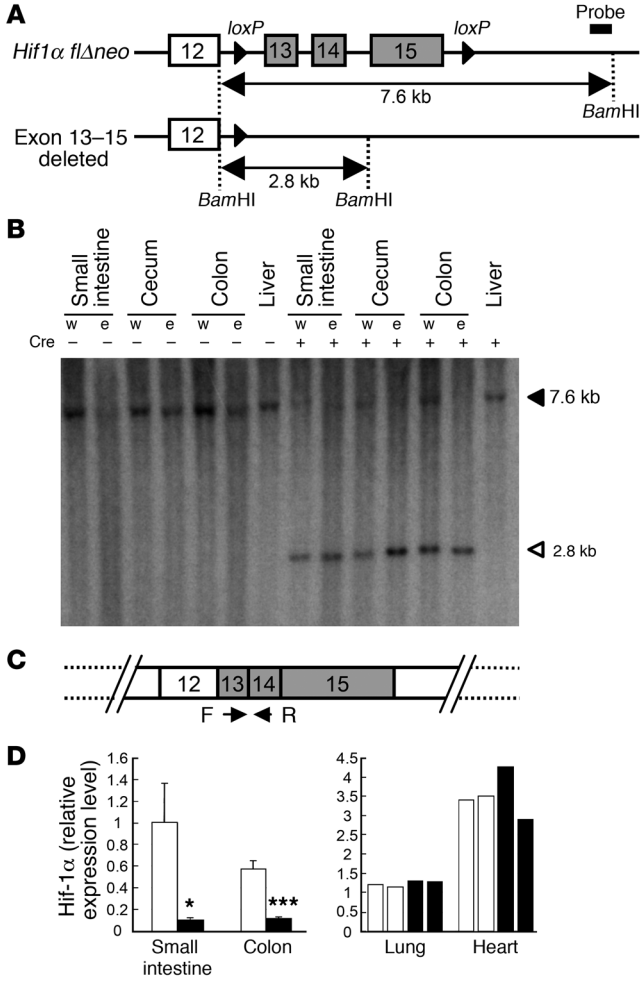

Figure 2
Intestinal epithelium–specific disruption of *Hif1a* gene. (**A**) Schematic structure of the modified *Hif1a* allele. The probe used in the Southern blot analysis is indicated. (**B**) Southern blot analysis for the *Hif1a* allele. Filled and open triangles indicate *Hif1a flΔneo* and exon 13–15–deleted allele, respectively (18). Fragments corresponding to the *Hif1a flΔneo* allele were only detected in Hif-1$\alpha^{\Delta IE}$ mice. w, whole tissue; e, epithelial cells. (**C**) Primers used for the detection of intact *Hif1a* transcripts. (**D**) Relative expression levels of the intact *Hif1a* transcripts measured by qPCR. White and black bars represent the Hif-1$\alpha^{F/F}$ and Hif-1$\alpha^{\Delta IE}$ mice, respectively. Average values for 4 mice (for intestine) or individual values in 2 mice (for lung and heart) in each group are shown. Relative values were calculated from the average expression level in the small intestine of the Hif-1$\alpha^{F/F}$ mice defined as standard (set as 1.0). Error bars indicate SEM. Statistical significance between the average of Hif-1$\alpha^{F/F}$ and Hif-1$\alpha^{\Delta IE}$ mice in the same tissue was examined. $^{*}P < 0.05$; $^{***}P < 0.001$.

breeding and dietary conditions; they were fertile, and their growth rate was comparable to that of the Arnt$^{F/F}$ mice. The structure of the intestine was histologically examined using paraffin sections stained with H&E, and there was no obvious difference between genotypes. In order to characterize the Arnt$^{\Delta IE}$ mice in more detail, global gene expression profiles were examined in the intestinal tract of Arnt$^{\Delta IE}$ and Arnt$^{F/F}$ mice by cDNA microarray analysis (data not shown). As expected, expression levels of the prototypical AhR target genes *Cyp1a1* and *Cyp1a2* were greatly reduced in Arnt$^{\Delta IE}$ mice compared with the control Arnt$^{F/F}$ mice. The expression of these genes was not eliminated but was dramatically reduced in the small intestine of the Arnt$^{\Delta IE}$ mice (Figure 3A). The differences in mRNA levels were also confirmed by Northern blot analysis (data not shown). The expression levels of CYP1A1 and CYP1A2 mRNA were extremely low in the cecum and colon, irrespective of genotype; thus, there were no clear differences in these regions in contrast to the small intestine, although a slight elevation in colon CYP1A1 mRNA expression was noted. Another AhR target gene, *Cyp1b1*, was also examined. Its expression was generally elevated in the intestine of Arnt$^{\Delta IE}$ mice, but the induction was statistically significant only in the cecum and colon (data not shown). The residual expression of the CYP1 enzymes in the intestinal tract of Arnt$^{\Delta IE}$ mice might be derived from the residual expression of the *Arnt* gene in nonepithelial tissues of the gut, where villin-Cre is not expressed.

The expression levels of typical Hif-1 target genes, *Vegf* and glucose transporter 1 (*Glut1*) (19), both expressed in the intestinal cells (20, 21), were not changed in the intestine of Arnt$^{\Delta IE}$ compared with Arnt$^{F/F}$ mice under normal breeding conditions, while a faint decrease was noted in the expression of egg-laying defective homolog 3 (*Egln3*), an Hif-1 target gene, in cultured cells (22) (data not shown). A marked induction of the metallothionein 1 (*Mt1*) gene throughout the intestinal tract was also noted (data not shown). Direct regulation of this gene through AhR/Arnt or Hif-1 has not previously been reported, although the induction was demonstrated in the livers of *AhR*-null mice (23). The *Mt1* expression was also highly elevated in the gut of Hif-1$\alpha^{\Delta IE}$ mice (data not shown). This suggests that *Mt1* induction in Arnt$^{\Delta IE}$ might be mediated by the loss of Hif-1 function in gut epithelium.

CYP1A1 expression levels and enzymatic activities are elevated in extra-gut tissues of Arnt$^{\Delta IE}$ mice. Quite surprisingly, CYP1A1 mRNA expression was elevated in almost all non-gut tissues examined. Among the tissues examined, lung, heart, tongue, and skeletal muscle showed the highest increases in mRNA expression (Figure 3B); there was no statistically significant difference in skin and spleen (Figure 3B). The difference in CYP1A1 mRNA expression between Arnt$^{F/F}$ and Arnt$^{\Delta IE}$ mice was reproducible in all littermate pairs examined in both sexes. It was recently demonstrated that 2-amino-1-methyl-6-phenylimidazo[4,5-*b*]pyridine (PhIP) is predominantly metabolized by CYP1A1 in the lung, yielding 2 major hydroxylated metabolites of PhIP, 4′-OH and N^2-OH PhIP (24). Using lung microsomes extracted from Arnt$^{F/F}$ and Arnt$^{\Delta IE}$ mice, we found PhIP hydroxylase activities to be dramatically increased in Arnt$^{\Delta IE}$ mice (Figure 3C). This suggests that not only mRNA expression but also enzymatic activities of CYP1A1 are markedly increased in non-gut tissues of the Arnt$^{\Delta IE}$ mice.

In order to determine whether the CYP1A1-inductive effect is present in embryos, CYP1A1 mRNA expression was examined in E7.5 embryos from pregnant Arnt$^{\Delta IE}$ females. To obtain both Arnt$^{\Delta IE}$ and Arnt$^{F/F}$ embryos within 1 litter, 2 types of mating pairs were designed: Arnt$^{\Delta IE}$ females with Arnt$^{F/F}$ males and Arnt$^{F/F}$ females with Arnt$^{\Delta IE}$ males. *Cyp1a1* expression levels were greatly increased in the embryos from Arnt$^{\Delta IE}$ mothers compared with those from Arnt$^{F/F}$ mothers; this was independent of the embryonic genotype (Figure 3D). However, it should be noted that the E7.5 embryos are still a mixture of embryonic and extraembryonic cells. Also, the placental tissues are not formed at this stage. Therefore, *Cyp1a1* induction could be specific for the very early-stage embryos.

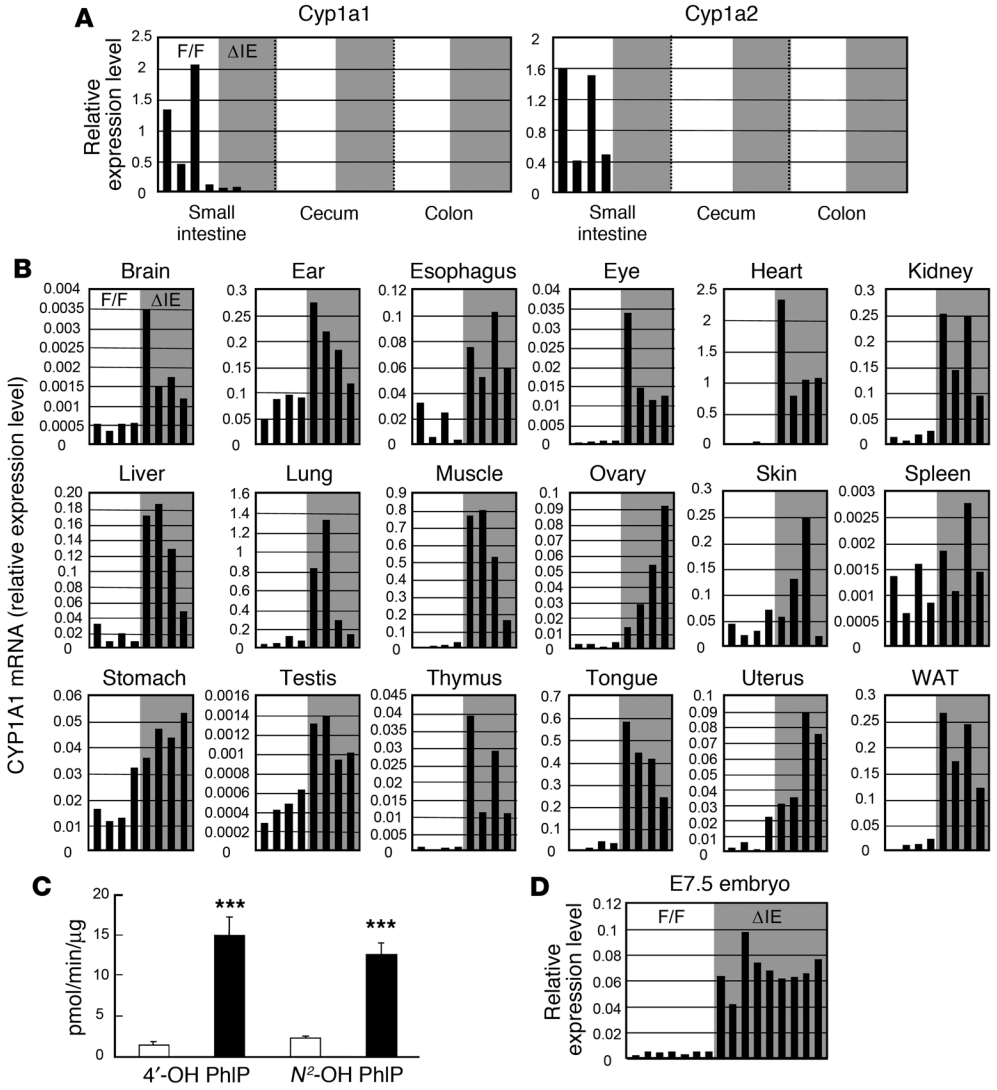

Figure 3

Gene expression profiles of Arnt$^{F/F}$ and Arnt$^{\Delta IE}$ mice under normal dietary conditions. (**A**) Expression levels of genes expressed in a genotype-dependent manner in the intestinal tract. Each bar corresponds to an individual animal. F/F, Arnt$^{F/F}$ (open); ΔIE, Arnt$^{\Delta IE}$ (shaded). (**B**) CYP1A1 mRNA expression levels in the various tissues. (**C**) PhIP hydroxylase activities in lung microsomes isolated from Arnt$^{F/F}$ and Arnt$^{\Delta IE}$ mice. Average values for each group (n = 6) are shown. White and black bars represent the expression levels in Arnt$^{F/F}$ and Arnt$^{\Delta IE}$ mice, respectively. (**D**) CYP1A1 mRNA expression levels in E7.5 embryos. Dams' genotypes are indicated. Each bar corresponds to an individual animal. A representative of 2 independent experiments is shown. mRNA expression levels were determined by qPCR. Relative values for each gene were calculated from the average expression level in the small intestine of the Arnt$^{F/F}$ mice with FVB/N background defined as general standard (set as 1.0). Error bars indicate SEM. Statistical significance between the average values for Arnt$^{F/F}$ and Arnt$^{\Delta IE}$ mice in the same tissue was examined. ***$P < 0.001$.

Indeed, it was previously reported that *Cyp1a1* expression in embryo was detectable only at 7.5 days post coitum, whereas it was almost undetectable at later developmental stages (25).

CYP1A1 induction in extra-gut tissues of Arnt$^{\Delta IE}$ mice is genetic background independent. The mouse *AhR* gene has polymorphic alleles yielding several isoforms of AhR protein that differ in binding affinity to AhR ligands. At least 4 types of AhR isoforms, Ah^{b1-3} and Ah^{d}, have been reported (26–28). Among these, Ah^{b1-3} have a higher binding affinity for AhR ligands such as BaP and 3-methylcholanthrene compared with that of the Ah^{d} isoform. Arnt$^{F/F}$ and villin-Cre mice were originally developed on the C57BL/6 background, which has the high-affinity Ah^{b1} isoform (13, 15). These mice were crossed onto the FVB/N background to generate the Arnt$^{\Delta IE}$ mice used in all of the present studies. This could potentially result in mixed AhR polymorphic alleles within our Arnt$^{\Delta IE}$ colonies. Thus, it was necessary to determine whether the difference in *Cyp1a1* expression was derived from the difference in genetic backgrounds or loss of Arnt function in gut.

For this purpose, CYP1A1 mRNA expression and enzymatic activities were examined in Arnt$^{F/F}$ and Arnt$^{\Delta IE}$ mice maintained in the original C57BL/6 background following 5 additional rounds of backcrossing to the C57BL/6N background. Indeed, the basal expression levels of *Cyp1a1* were generally high in the C57BL/6N background irrespective of the genotype (Figure 4A). Expression was especially high in the lung (Figure 4A). However, CYP1A1 mRNA expression and enzymatic activities in extra-gut tissues were significantly elevated in Arnt$^{\Delta IE}$ mice even on the C57BL/6N background (Figure 4, A and B). This was confirmed in all littermate pairs examined. Although lung enzymatic activities did not exactly parallel the mRNA expression in our system, the induction of both enzymatic activity and mRNA expression was always robust. These results clearly indicate that CYP1A1 induction in Arnt$^{\Delta IE}$ mice was caused by the loss of Arnt function in gut epithelium rather than by differences in genetic background.

Extra-gut P450 induction in Arnt$^{\Delta IE}$ mice is CYP1A1 selective, dietary factor dependent, and Hif-1α independent. Besides CYP1A1, other P450 enzymes, such as CYP1A2 and CYP1B1, are also under control of the AhR (29). Thus, the expression levels of these genes in various non-gut tissues were measured. CYP1A2 mRNA was predominantly expressed in the liver, as already reported (25). The expression was slightly elevated in Arnt$^{\Delta IE}$ compared with Arnt$^{F/F}$ mice in this tissue (Figure 4C). On the other hand, CYP1A2 mRNA expression

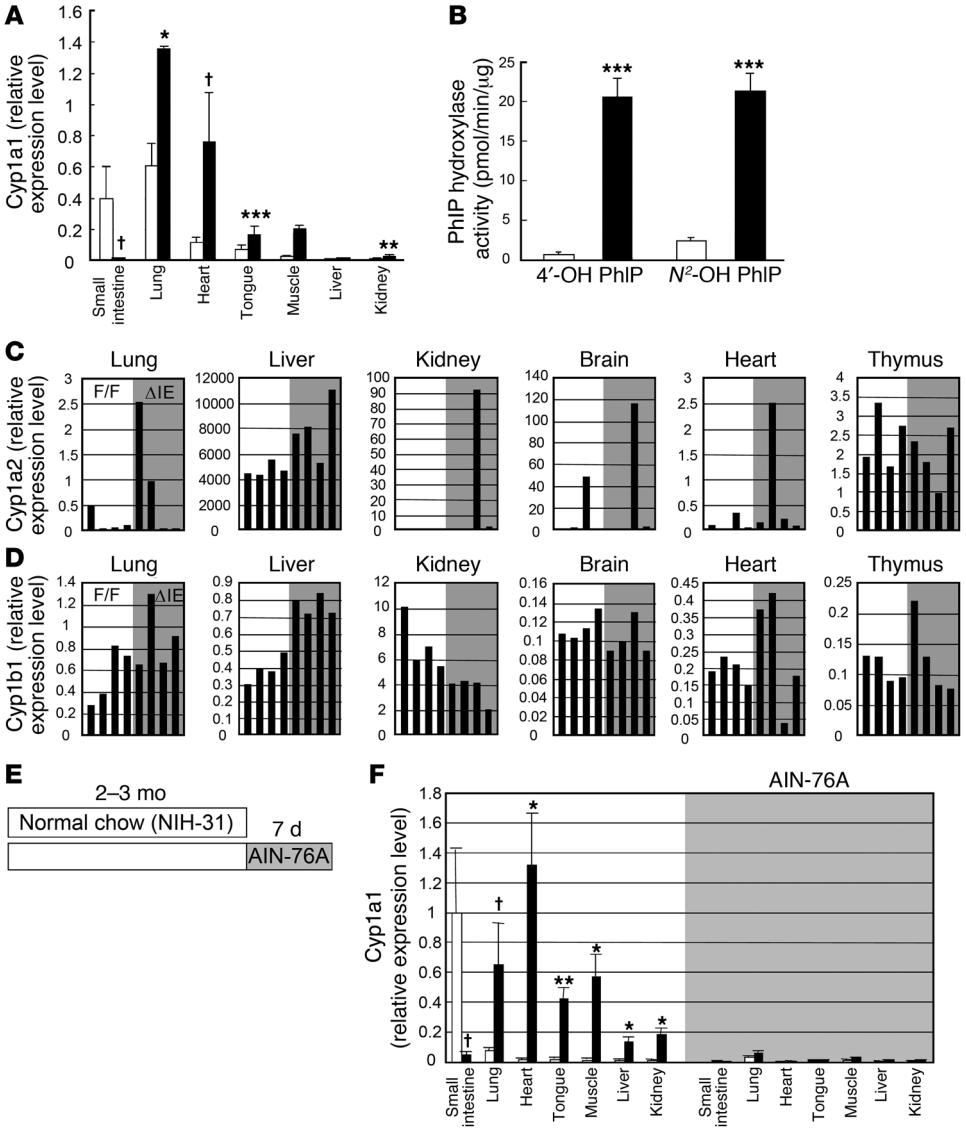

Figure 4
Genetic background independency, gene selectivity, and dietary factor dependency of the extra-gut P450 induction in Arnt$^{\Delta IE}$ mice. (**A**) Cyp1a1 expression levels in Arnt$^{F/F}$ and Arnt$^{\Delta IE}$ mice on the C57BL/6N background. Average values for each group (n = 4) are shown. White and black bars represent the expression levels in Arnt$^{F/F}$ and Arnt$^{\Delta IE}$ mice, respectively. (**B**) PhIP hydroxylase activities of lung microsomes isolated from Arnt$^{F/F}$ and Arnt$^{\Delta IE}$ mice on the C57BL/6N background. Average values for each group (n = 4) are shown. White and black bars represent the expression levels in Arnt$^{F/F}$ and Arnt$^{\Delta IE}$ mice, respectively. (**C** and **D**) mRNA expression levels of Cyp1a2 (**C**) and Cyp1b1 (**D**) in Arnt$^{F/F}$ and Arnt$^{\Delta IE}$ mice. Each bar corresponds to an individual animal. F/F, Arnt$^{F/F}$ (open); ΔIE, Arnt$^{\Delta IE}$ (shaded). (**E**) Diet administration scheme. (**F**) Cyp1a1 mRNA expression levels before (white) and after (shaded) the administration of the purified diet. Average values for each group (n = 3–4) are shown. mRNA expression levels were determined by qPCR. Relative values for each gene were calculated from the average expression level in the small intestine of the Arnt$^{F/F}$ mice on the FVB/N background defined as general standard (set as 1.0). Error bars indicate SEM. Statistical significance between the average values for Arnt$^{F/F}$ and Arnt$^{\Delta IE}$ mice in the same tissue under the same dietary conditions was examined. $^{*}P < 0.05$; $^{\dagger}P < 0.05$; $^{**}P < 0.005$; $^{***}P < 0.001$.

was extremely low in other nonhepatic tissues, showing large individual variation independent of the genotype (Figure 4C). CYP1B1 mRNA levels were constant in extra-gut tissues, although a slight induction in the liver and a reduction in the kidney were noted in Arnt$^{\Delta IE}$ mice (Figure 4D). These data suggest that the dramatic induction is specific for CYP1A1.

Ingredients of vegetable origin such as alfalfa meal are found in the NIH-31 diet normally used for breeding animals. Vegetables generally contain potential AhR ligands or P450 inducers, typically flavonoids and indoles (30, 31). Since the AhR signal transduction pathway is impaired in the gut, an AhR ligand in the diet might influence the phenotype of Arnt$^{\Delta IE}$ mice. To clarify the relationship between dietary factors and the extra-gut CYP1A1 induction, the diet was switched to a synthetic purified diet that contains fewer potent AhR ligands (AIN-76A diet). Arnt$^{\Delta IE}$ and Arnt$^{F/F}$ mice fed normal chow for the first 2–3 months of life were administered the AIN-76A diet for 1 week and CYP1A1 mRNA expression levels examined in various tissues (Figure 4E). Overall, the basal *Cyp1a1* expression levels were greatly reduced, and the statistically significant induction was lost in Arnt$^{\Delta IE}$ mice (Figure 4F). These results indicate the CYP1A1 induction in non-gut tissues of Arnt$^{\Delta IE}$ mice is dietary factor dependent.

Arnt plays critical roles in AhR-mediated and Hif-1α–mediated pathways (5, 6, 12). To clarify whether extra-gut CYP1A1 induction is mediated through Hif-1α in gut, *Cyp1a1* expression levels were examined in non-gut tissues of Hif-1α$^{\Delta IE}$ mice. No increased expression of CYP1A1 mRNA was noted in the lung and heart of the Hif-1α$^{\Delta IE}$ mice (data not shown). This strongly indicates that the machinery responsible for the CYP1A1 induction is independent of the Hif-1–mediated pathways in the intestine.

The expression levels of AhR and Arnt mRNAs in various tissues were also examined. No genotype-dependent difference was found in the expression levels of these genes in extra-gut tissues (Figure 1D). Therefore, Arnt or AhR mRNA expression levels are not the direct cause of the *Cyp1a1* induction in non-gut tissues.

Dietary phytochemicals potentate CYP1A1 induction in non-gut tissues of Arnt$^{\Delta IE}$ mice. Because of the complexity of natural ingredients in the NIH-31 diet, it is difficult to determine the exact nature of the

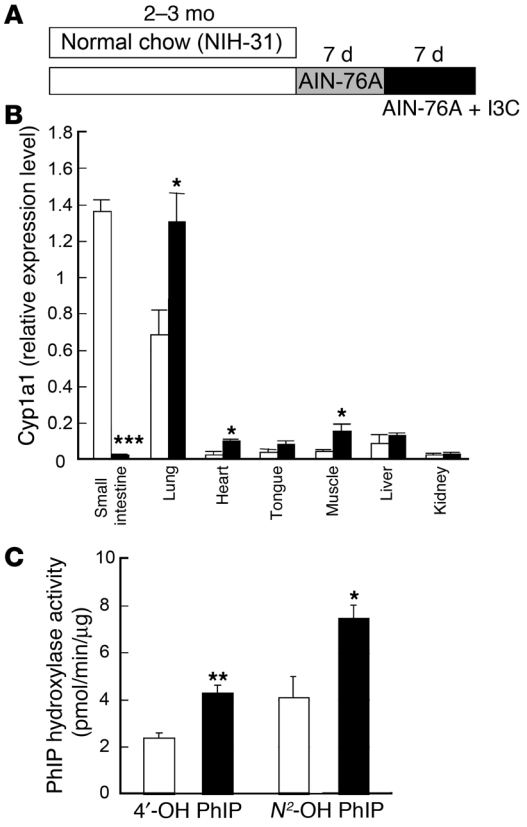

Figure 5
Effect of I3C administration on CYP1A1 expression and enzymatic activities. (**A**) Diet administration scheme. (**B**) Cyp1a1 mRNA expression levels in various tissues after administration of the AIN-76A diet supplemented with I3C. White and black bars represent the expression levels in $Arnt^{F/F}$ and $Arnt^{\Delta IE}$ mice, respectively. Three mice per each group were examined. mRNA expression levels were determined by qPCR. Relative values were calculated from the average expression levels in the small intestine of the $Arnt^{F/F}$ mice on the FVB/N background defined as general standard (set as 1.0). (**C**) PhIP hydroxylase activities of lung microsomes isolated from $Arnt^{F/F}$ and $Arnt^{\Delta IE}$ mice. The average results for 3 mice per each group are shown. White and black bars represent the expression values in $Arnt^{F/F}$ and $Arnt^{\Delta IE}$ mice, respectively. Error bars indicate SEM. Statistical significance between the average values for $Arnt^{F/F}$ and $Arnt^{\Delta IE}$ mice in the same tissue under the same dietary conditions was examined. $^{*}P < 0.05$; $^{**}P < 0.005$; $^{***}P < 0.001$.

chemicals responsible for the extra-gut CYP1A1 induction. However, it was suspected that one or more phytochemicals in the diet might be responsible for the induction. To examine this hypothesis, a proof-of-concept experiment was conducted. A phytochemical, I3C, was administered to $Arnt^{\Delta IE}$ mice through dietary supplementation. I3C and its precursor are widely distributed among cruciferous vegetables such as broccoli, cabbage, and cauliflower. It is believed that I3C has a variety of favorable effects on human health, including chemoprevention, although the exact mechanism is not fully understood (32, 33). It is also known that one of the major I3C metabolites, indolo[3,2-b]carbazole (ICZ), exhibits a high affinity for the AhR, inducing CYP1A1 activity (34).

As already shown, upon administration of the AIN-76A diet, *Cyp1a1* expression was greatly reduced irrespective of genotype (Figure 4F). However, when we administered the AIN-76A diet supplemented with I3C, *Cyp1a1* expression was recovered in both $Arnt^{F/F}$ and $Arnt^{\Delta IE}$ mice. More importantly, CYP1A1 mRNA expression and enzymatic activities were significantly elevated in $Arnt^{\Delta IE}$ mice (Figure 5). These results demonstrate that a dietary phytochemical can potentiate the extra-gut CYP1A1 induction in $Arnt^{\Delta IE}$ mice. However, since the tissue-dependent patterns of *Cyp1a1* expression differ from those observed under NIH-31–fed conditions, the factor(s) responsible for the CYP1A1 induction under normal dietary conditions is not likely to be I3C itself. Indeed, when the composition of the NIH-31 diet was examined using liquid chromatography–mass spectrometry (LC-MS), neither I3C nor its metabolites were detected, although these ions were readily detectable in the AIN-76A diet supplemented with I3C (data not shown).

I3C metabolism in gut epithelium is altered in $Arnt^{\Delta IE}$ mice. The fact that I3C supplementation in the AIN-76A diet could largely mimic the effect of the NIH-31 diet validated the conclusion that phytochemical components in NIH-31 diet were responsible for inducing CYP1A1 expression in the non-gut tissues of $Arnt^{\Delta IE}$ mice. Under I3C-fed condition, it is possible that altered I3C metabolism in the intestine of $Arnt^{\Delta IE}$ mice led to the accumulation of I3C or its derivatives and therefore was responsible for the extra-gut CYP1A1 induction. To examine this hypothesis, the metabolic profiles of I3C in the urine and fecal extracts of $Arnt^{\Delta IE}$ and $Arnt^{F/F}$ mice were globally examined using an LC-MS–based metabolomic approach, since multivariate data analysis (MDA), the data processing platform of metabolomics, is able to detect subtle differences in a large dataset. Each urine or fecal sample was characterized by its intrinsic chemical species, separated by ultra-performance liquid chromatography (UPLC), and detected by a time-of-flight mass spectrometer (TOFMS). The retention time, accurate mass, and intensity of each ion species were then compiled to construct the multivariate data matrix. Following data processing, the relationship among samples can be defined and the ions contributing this relationship can be further identified (35).

Using the partial least-squares discriminant analysis (PLS-DA) method (35), in which samples were classified based on dietary conditions and genotypes, data from urine and fecal samples from $Arnt^{\Delta IE}$ and $Arnt^{F/F}$ mice were grouped according to the 3 dietary conditions (Figure 6, A and B). Then, under the same dietary condition, results for urine and feces of $Arnt^{\Delta IE}$ and $Arnt^{F/F}$ mice were also distinctively grouped in the scores plot, although the genotype-dependent differences were not as prominent as the diet-dependent differences (Figure 6, A and B). Ions with m/z 130^+ and 334^+ were found to be the greatest contributors for the separation of I3C-fed $Arnt^{\Delta IE}$ mice from the other groups in both urine and fecal extracts (Figure 6, C and D), and the relative abundance of both ions was significantly higher in $Arnt^{\Delta IE}$ mice compared with $Arnt^{F/F}$ mice (Figure 6, E and F). Since tandem mass spectrometry (MS/MS) fragmentation of ion 334^+ yielded a major fragment ion with m/z 130^+ (data not shown) and both ions had the same retention time (~4.8 minutes), ion 130^+ is an in-source fragment of ion 334^+ generated by the ionization process in the mass spectrometer. Chemical identity of ion 130^+ was defined as a dehydrated I3C ion based on the accurate mass–derived molecular formula ($C_9H_8N^+$, a loss of H_2O from $C_9H_{10}NO^+$, the protonated I3C ion) and the fact that MS/MS fragmentation of the I3C standard generated ion 130^+ (data not shown). The exact chemical structure of ion 334^+ was not resolved in this study, although its identity as a metabolite of I3C was supported by

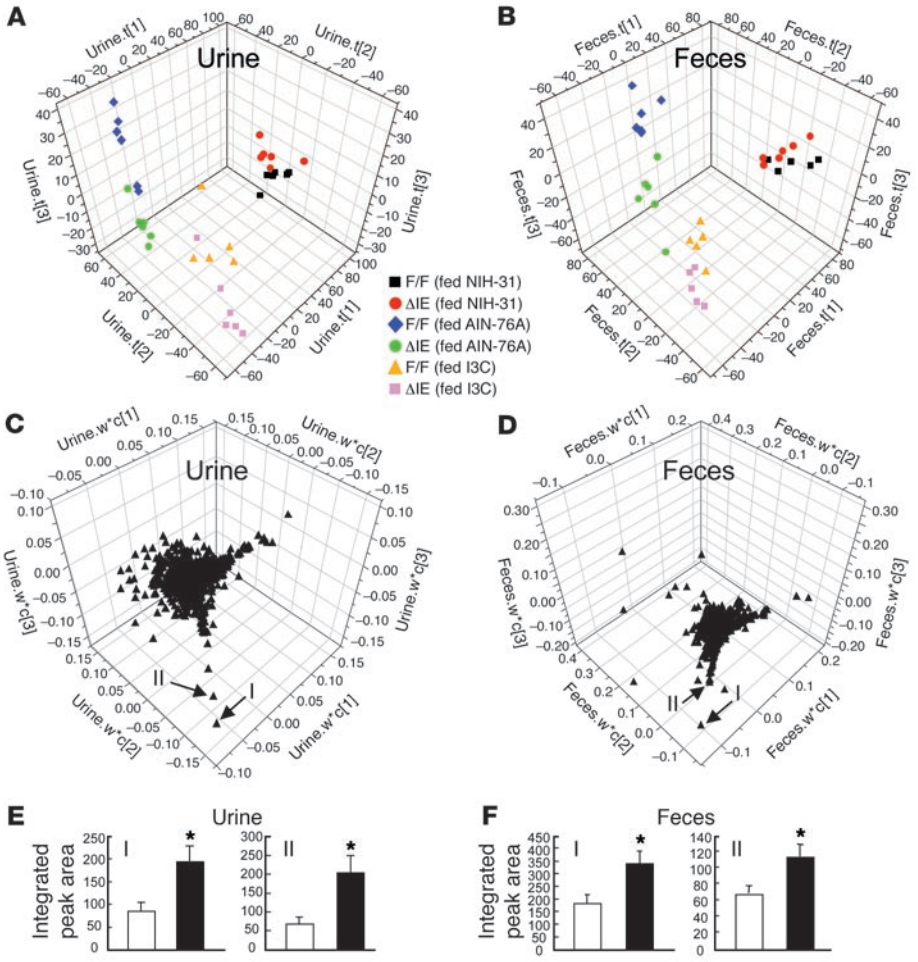

Figure 6
Metabolomic analysis of urine and fecal extracts from I3C-fed animals. The results of PLS-DA for urine and fecal extracts. Three components were assigned to build up these models by SIMCA-P+ 11 software in each case. (**A**) The 3D scores scatter plots for urine. Individual samples are scattered depending on their compositions. The t[1], t[2], and t[3] values represent the contribution scores of each sample in components 1, 2, 3, respectively. Corresponding symbols and colors for the genotype and dietary conditions of each sample are indicated. F/F, $Arnt^{F/F}$; ΔIE, $Arnt^{\Delta IE}$. (**B**) The 3D scores scatter plots for fecal extracts. (**C**) The 3D loading scatter plots for urine. Each triangle indicates an individual ion distributed depending on its contribution to each component. The w*c[1], w*c[2], and w*c[3] values represent the contribution scores of each ion for components 1, 2, and 3, respectively. (**D**) The 3D loading scatter plots for fecal extracts. I: ion with *m/z* 130^+ and retention time approximately 4.8 minutes; II: ion with *m/z* 334^+ and retention time approximately min. Average integrated peak areas for ions I and II in urine (**E**) and fecal extracts (**F**) are also shown. White and black bars represent the values in $Arnt^{F/F}$ and $Arnt^{\Delta IE}$ mice, respectively. Five to 6 mice per each group were examined. Error bars indicate SEM. Statistical significance between the average values for $Arnt^{F/F}$ and $Arnt^{\Delta IE}$ mice in the same sort of samples under the same dietary conditions was examined. *$P < 0.05$.

several pieces of evidence: (a) ion 334^+ was detected only in I3C-fed mice and not in the mice fed the NIH-31 or AIN-76A diet alone; (b) MS/MS fragmentation of ion 334^+ yielded *m/z* 130^+ as a major daughter ion; and (c) I3C is known for its complex oligomerization reactions under acidic conditions (such as those found in the stomach), which can generate multiple I3C derivatives with PAH structures (36). Although the molecular mass of this ion did not match any reported I3C metabolites and derivatives, it is highly possible that this ion originated from the oligomerized I3C.

In addition to these 2 ions, a number of ions were found to contribute to the separation of I3C-fed $Arnt^{\Delta IE}$ mice samples from other groups. The relative abundance of these ions was elevated with statistical significance in the urine or feces of I3C-fed $Arnt^{\Delta IE}$ mice (data not shown). Importantly, all of these ions were detected only under the I3C-fed conditions. Also, like the ion 334^+, most of these ions yielded a fragment of *m/z* 130^+, the dehydration product of I3C, in the fragmentation analysis, suggesting that they were derived from the I3C in the diet. Differences in the levels of the I3C metabolites were observed in both urine and fecal extracts, with greater differences in urine (Figure 6). Since the fecal output is directly governed by a local metabolism in gut, it was suggested that the I3C metabolism in gut was significantly altered in $Arnt^{\Delta IE}$ mice.

Discussion

Despite its role in the metabolic activation of PAH carcinogens (6, 29), CYP1A1 also functions as a detoxifying enzyme, since CYP1A1-mediated reactions expedite the elimination of many xenobiotics, especially in extrahepatic tissues (37). Because of this potential influence on the subtle balance between bioactivation and detoxification, CYP1A1 expression should be tightly regulated according to the circumstances. The current study, using an intestine-specific *Arnt*-knockout mouse model, provides the first evidence to our knowledge showing the existence of a dietary phytochemical–mediated intestinal regulatory pathway that controls whole-body CYP1A1 expression. Since *villin* is also expressed in the kidney cortex and extraembryonic visceral endoderm, Cre recombinase expression in these tissues might be relevant to the local phenomenon observed in $Arnt^{\Delta IE}$ mice to some extent (15). However, the protein expression and activity of the Cre recombinase was significantly lower in the kidney of villin-Cre mice compared with the intestinal epithelium (15); indeed, exon 6–deleted *Arnt* allele was not detected in the kidney of $Arnt^{\Delta IE}$ mice by Southern blot analysis (Figure 1B). It should also be noted that extra-gut CYP1A1 induction was observed in almost all tissues of adult mice of both sexes. These observations strongly suggest that loss of Arnt expression in the intestinal epithelium was the primary cause of the whole-body phenotype observed in $Arnt^{\Delta IE}$ mice.

There are at least 2 possible explanations for the observed CYP1A1 induction in extra-gut tissues of $Arnt^{\Delta IE}$ mice. The first

hypothesis is that in Arnt$^{\Delta IE}$ mice, certain dietary CYP1A1 inducers can pass through the intestine in their active or original forms and enter peripheral tissues to induce *Cyp1a1* expression, while in the Arnt$^{F/F}$ mice these phytochemicals are deactivated by target gene products from an intact Arnt/AhR system. The second hypothesis is that specific *Cyp1a1*-suppressive factors that are normally released from the gut of Arnt$^{F/F}$ mice might be lost or attenuated in Arnt$^{\Delta IE}$ mice. While the latter mechanism can explain the extra-gut CYP1A1 induction in Arnt$^{\Delta IE}$ mice, it cannot explain the observation that the CYP1A1 expression levels remain considerably higher in the intestine of Arnt$^{F/F}$ mice in comparison to other tissues.

To examine the first hypothesis, which focuses on the presumptive CYP1A1 inducer(s), a LC-MS–based metabolomic approach was adopted to distinguish the metabolism profiles of Arnt$^{F/F}$ and Arnt$^{\Delta IE}$ mice fed the NIH-31 diet; although a multivariate model encompassing both urinary metabolomes of Arnt$^{F/F}$ and Arnt$^{\Delta IE}$ mice could be established, the genotype-dependent differences presented by the model were very subtle and could not provide enough information for the identification of potential dietary *Cyp1a1* inducers. It is possible that the amounts of potential *Cyp1a1* inducers were very low or nonexistent in the urine or the LC-MS condition used in this study was not optimized for these chemicals.

Because of the difficulty in identifying potential natural CYP1A1 inducers in the NIH-31 diet, a proof-of-concept experiment using I3C, a known CYP1A1 inducer, was conducted. I3C administration through dietary supplementation could largely mimic the extra-gut CYP1A1 induction in Arnt$^{\Delta IE}$ mice. Metabolomic analysis of urine and fecal samples further showed that the intestinal metabolism of I3C in Arnt$^{\Delta IE}$ mice was different from its metabolism in Arnt$^{F/F}$ mice. In fact, the grouping of the results for I3C-treated Arnt$^{\Delta IE}$ and Arnt$^{F/F}$ samples was attributed to the higher abundance of I3C derivatives, such as ion 334^{+}, in Arnt$^{\Delta IE}$ than Arnt$^{F/F}$ mice. It is highly plausible that some of I3C derivatives expressed at high levels in Arnt$^{\Delta IE}$ mice, due to the altered AhR/Arnt-dependent metabolism in the gut, are responsible for the extra-gut CYP1A1 induction under I3C treatment. Although I3C itself was not detected in the LC-MS analysis of chemical components of the NIH-31 diet, a similar mechanism can still be applicable to explain the extra-gut CYP1A1 induction in the Arnt$^{\Delta IE}$ mice, since the NIH-31 diet contains other natural CYP1A1 inducers derived from plants, such as flavonoids and carotenoids (30, 31, 38). Overall, these results suggest that an Arnt- and a phytochemical-dependent system in the gut plays an important role in the elimination or reduction of circulating natural AhR ligands and the suppression of whole-body CYP1A1 expression. Interestingly, despite the fact that all CYP1 enzymes are regulated through AhR/Arnt, only CYP1A1 expression was dramatically induced in Arnt$^{\Delta IE}$ mice. A possible explanation is that there may exist differential tissue-selective regulatory mechanisms that control the basal expression of CYP1A1 and other CYP1 enzymes.

Recently, the conventional view on the role of CYP1A1 in the metabolic activation and detoxification of PAH procarcinogens was challenged by a series of studies (7, 37, 39). Numerous in vitro studies using recombinant CYP1A1 enzyme, microsomes, and hepatocytes in combination with chemical inhibitors of CYP1A1 have provided strong evidence that CYP1A1 possesses the highest catalytic activity among P450 enzymes with regard to the generation of genotoxic metabolites of PAHs (5, 6). Thus, it became widely accepted that CYP1A1 is the primary enzyme responsible for the toxicity of PAHs. Based on this theory, mice deficient in CYP1A1 should be resistant to BaP treatment. However, when challenged with BaP, unexpectedly, *Cyp1a1*-null mice were much more susceptible to the BaP-induced toxicity and DNA adduction in comparison with wild-type *Cyp1a1*$^{+/+}$ mice (7). This observation suggested that in the intact mouse, sustaining an appropriate level of CYP1A1 is beneficial, rather than detrimental, to the cytoprotective function against environmental toxins, even though the underlying mechanism behind this phenomenon is still largely unknown (9).

One interesting observation in the current study was that the CYP1A1 mRNA expression in non-gut tissues was almost undetectable in mice on the FVB/N background, while its level was considerably higher in mice on the C57BL/6N background. Indeed, the highest CYP1A1 expression was detected in the lung of the mice on the C57BL/6 background (24). It was reported that FVB/N mice are highly susceptible to chemical-induced carcinogenesis in lung, mammary gland, and skin, while C57BL/6 mice are resistant (40–43). This correlation was consistent with the suggested in vivo protective function of CYP1A1, although other genetic differences between the 2 mouse strains may also contribute to the discrepancy in cancer susceptibility.

Like the C57BL/6 strain and *Cyp1a1*$^{+/+}$ mice in comparison to the FVB/N strain and *Cyp1a1*-null mice, the Arnt$^{\Delta IE}$ mice sustain higher CYP1A1 expression in peripheral tissues compared with the control Arnt$^{F/F}$ mice. Thus, the in vivo chemopreventive function of CYP1A1 as shown in recent articles (7, 37, 39) suggests that the Arnt$^{\Delta IE}$ mice might be more resistant to chemically induced carcinogenesis, in addition to having an overall resistance to nongenomic toxicity from xenobiotics. However, this should be confirmed by careful examination of a wide variety of carcinogens and/or procarcinogens by multiple routes of administration, since the effect on carcinogenesis would be different depending on the particular chemical and means of exposure.

This system could play an important role not only in carcinogenesis but also in various aspects of biological responses to external stimuli. Interestingly, in addition to the non-gut tissues, *Cyp1a1* expression was also strongly upregulated in early-stage embryos in pregnant Arnt$^{\Delta IE}$ females. The CYP1A1 substrates, such as 2,3,7,8-tetrachlorodibenzo-*p*-dioxin (TCDD) and BaP, are highly teratogenic in utero (44, 45). Besides, these toxins elicit fetal/neonatal death or carcinogenesis. Recently, it was reported that administration of I3C to pregnant females greatly reduces the risk of transplacental carcinogenesis by BaP through a largely unknown mechanism (46). If this was attributable to the elevated CYP1A1 expression induced by I3C in utero, fetus of Arnt$^{\Delta IE}$ females might be protected from the toxic effects of PAHs due to increased CYP1A1 activity. Another role for this system might be in protection against environmental hormone-like substances (endocrine disruptors). It was demonstrated that bisphenol A (BPA), a material widely used in plastic wares, is metabolized by CYP1A1 (47). This chemical, as a major environmental hormone mimic, influences embryonic development, sexual maturity, and carcinogenesis (48). Thus, CYP1A1 induction might be important for maintaining proper development in utero and overall protection from the unfavorable effects of endocrine disruptors in the environment.

Identification of the phytochemical-mediated regulatory mechanism in this study provides insights into the role of the intestinal AhR/Arnt system in xenobiotic metabolism. Metabolomic analysis of I3C-treated animals further suggested that intestinal metabolism of xenobiotics could significantly affect CYP1A1 expression

in non-gut tissues. Others demonstrated that the nongenomic toxicity of BaP in mice was markedly different depending on whether administration was oral or intravenous (7). Interestingly, *Cyp1a1*$^{+/+}$ mice were more resistant to oral administration of BaP than *Cyp1a1*-null mice; however, when *Cyp1a1*$^{+/+}$ mice were given an intraperitoneal injection of BaP, their survival rate dramatically dropped to levels comparable to those of *Cyp1a1*-null mice (7). This also indicates the significant contribution of the intestine to the detoxification of harmful xenobiotics through the direct local metabolism to the whole-body-level metabolism.

Together, the results from this study revealed an Arnt- and phytochemical-dependent intestinal system that regulates whole-body CYP1A1 expression. Since plant-derived food is the major source of natural CYP1A1 inducers, it is reasonable to suspect that the composition of the daily diet can affect xenobiotic metabolism in the body through this regulatory system. Furthermore, this system can also be considered as a target for developing new chemopreventive agents and therapeutic entities.

Methods

Animals and diets. Mice homozygous for a modified *Arnt* allele in which exon 6 is flanked by *loxP* sites (*Arnt flΔneo*) (13), originally developed on a C57BL/6 background, were backcrossed into the FVB/N background for 5 generations to obtain *Arnt flΔneo* homozygous mice on an FVB/N background (designated Arnt$^{F/F}$ mice in this work). These mice were then mated with villin-Cre mice (15) backcrossed to the FVB/N background to produce Arnt$^{F/F}$ mice carrying the villin-Cre transgene on the FVB/N background (designated Arnt$^{\Delta IE}$ mice). Arnt$^{F/F}$ and Arnt$^{\Delta IE}$ mice on the FVB/N background were used in all experiments unless otherwise noted. For analyses on the C57BL/6 background, Arnt$^{F/F}$ and Arnt$^{\Delta IE}$ mice were further backcrossed 5 times to C57BL/6N mice. Similarly, mice homozygous for a modified *Hif1a* allele in which exons 13–15 are flanked by *loxP* sequences (*Hif1a flΔneo*; ref. 18) (designated Hif-1α$^{F/F}$ mice in this study) were mated with villin-Cre mice to generate mice carrying homozygous *Hif1a flΔneo* allele and villin-Cre transgene (designated Hif-1α$^{\Delta IE}$ mice). All mice with the modified *Hif1a* allele were maintained on the C57BL/6 background. Mice were fed a normal diet (Rodent NIH-31 Auto 18-4; Zeigler), synthetic purified diet (AIN-76A Rodent diet; Bio-Serv), or the purified diet supplemented with 2,000 ppm of I3C, under 12-hour light/12-hour dark cycles. I3C was purchased from Sigma-Aldrich. Food and water were provided ad libitum. Mice were killed by CO_2 asphyxiation. Mice fed synthetic purified and I3C-containing diets were killed on day 7 of the treatment. Tissue samples were collected, frozen in liquid nitrogen, and stored at –80°C until further analysis. Protocols for all animal studies were approved by the National Cancer Institute Animal Care and Use Committee and were carried out in accordance with the guidelines of Institute of Laboratory Animal Resources.

Genotype determination. For Southern blot analysis, tissues from 2- to 3-month-old mice were digested with proteinase K, phenol/chloroform extracted, and genomic DNA was precipitated with 2-propanol. Ten micrograms of each sample was digested with *Bam*HI, separated on a 0.6% agarose-Tris-acetate-EDTA gel, and transferred to a nylon membrane. Membranes were hybridized with the probes indicated in Figure 1A (for Arnt) and Figure 2A (for Hif-1α) as described in previous reports (13, 18). Routine genotyping for the Arnt allele was performed with PCR primers Arnt-F4, 5′-ACGCACTACAACACCTGAGCTAA-3′, and Arnt-R4, 5′-GCATGCTGGCACATGCCTGTCT-3′, to discriminate the Arnt floxed allele (~0.7 kb) from the wild-type allele (~0.6 kb) by the difference in amplified DNA fragments. Routine genotyping for the Hif-1α allele was performed with 3 PCR primers, H1–3, described in a previous report (18). The existence of the Cre transgene was determined by a mixture of 4 PCR primers: Cre-F: 5′-AGGTGTAGAGAAGGCACTTAGC-3′; Cre-R: 5′-CTAATCGCCATCTTCCAGCAGG-3′; MEH-F8: 5′-AAGTGAGTTTGCATGGCGCAGC-3′; MEH-R8: 5′-CCCTTTAGCCCCTTCCCTCTG-3′. MEH-F8 and MEH-R8 amplify a sequence specific for the microsomal epoxide hydroxylase (mEH) gene and were used as positive controls.

RNA extraction and qRT-PCR analysis. Total RNA samples were extracted from 2- to 3-month-old mice using TRIzol reagent (Invitrogen), and 3-μg aliquots were reverse transcribed. qPCR analysis was performed using ABI PRISM 7900HT Sequence Detection System (Applied Biosystems) with SYBR green chemistry. Relative expression levels were determined by the ΔΔCt (comparative Ct) method using β-actin mRNA expression levels as an internal control. Relative expression levels were further normalized by defining the average expression level of each gene in the small intestine of Arnt$^{F/F}$ (FVB/N) mice (for the analysis of Arnt$^{F/F}$ and Arnt$^{\Delta IE}$ mice) or Hif-1α$^{F/F}$ mice (for the analysis of Hif-1α$^{F/F}$ and Hif-1α$^{\Delta IE}$ mice) fed a normal chow diet as 1.0. Primers were designed using Primer Express 2.0.2 software (Applied Biosystems) and validated by homology search by nucleotide BLAST (http://nciarray.nci.nih.gov/), while other primers were described in an earlier report (49). Primer sequences used were as follows (gene symbol: forward, reverse): Arnt: 5′-CAAGCCATCTTTCCTCACTGATC-3′, 5′-ACACCACCCGTCCAGTCTCA-3′; AhR: 5′-CGGCTTCTTGCAAAACACAGT-3′, 5′-GTAAATGCTCTCGTCCTTCTTCATC-3′ (49); Hif-1α: 5′-ATAGCTTCGCAGAATGCTCAGA-3′, 5′-CAGTCACCTGGTTGCTGCAA-3′; Cyp1a1: 5′-GGTTAACCATGACCGGGAACT-3′, 5′-TGCCCAAACCAAAGAGAGTGA-3′; Cyp1a2: 5′-GGAGAATGTCACCTCAGGGAAT-3′, 5′-CGAAGTTATCATTGAAGGTCTTAAACC-3′; Cyp1b1: 5′-CCCCCCAAAACAAAAACAGAT-3′, 5′-AGAGTGTGCTAATATTTCACAGGTCAA-3′; Egln3: 5′-GTCCCGTGGCTCAGTTTTGT-3′, 5′-GGCATCACAGGCTAAAGAGACA-3′; Mt1: 5′-CCAGGGCTGTGTCTGCAAA-3′, 5′-TGGGTTGGTCCGATACTATTTACA-3′; β-actin: 5′-TATTGGCAACGAGCGGTTCC-3′, 5′-GGCATAGAGGTCTTTACGGATGTC-3′.

cDNA microarray analysis. Equal amounts of total RNA samples extracted from the small intestine, cecum, and colon of 4 mice in each of the Arnt$^{F/F}$ and Arnt$^{\Delta IE}$ groups were pooled in each tissue for comparison. In addition, in the case of the small intestine, total RNA samples from individual Arnt$^{F/F}$ and Arnt$^{\Delta IE}$ littermates were compared in independent experiments. Two- to 3-month-old mice fed the normal diet were used for analyses. Amino-modified cDNAs were synthesized from 20 μg of each pooled or individual RNA samples using the SuperScript Indirect cDNA Labeling Kit (Invitrogen) after the pre–clean-up through an RNeasy Mini column (QIAGEN). Synthesized amino-modified cDNAs were purified with MinElute PCR Purification Kit (QIAGEN), and cDNAs synthesized from the RNA of Arnt$^{F/F}$ and Arnt$^{\Delta IE}$ mice were coupled with Cy3 (for Arnt$^{F/F}$) and Cy5 (for Arnt$^{\Delta IE}$) fluorescent dyes (Amersham Biosciences). Dye-coupled cDNAs were purified with a MiniElute PCR purification kit (QIAGEN) and hybridized to the National Cancer Institute in-house–printed oligonucleotide DNA spotted glass slides (Mouse Exotic Evidence Based Oligonucleotide [MEEBO] Set; Gene Expression Omnibus [GEO] accession number GPL4200). Hybridized slides were washed, scanned, and analyzed using a GenePix 4000A scanner and GenePix Pro 3.0 software (Axon Instruments). A detailed protocol has been published elsewhere (50). Datasets were further analyzed by a microarray database (mAdb) system provided by the NIH Center for Information Technology. Expression levels of the genes exhibiting significant genotype-dependent difference were validated individually by qPCR.

UPLC-TOFMS analysis of biological fluids. Urine and feces were collected from 2- to 3-month-old male mice for 24 hours using metabolic cages. For animals fed AIN-76A– and I3C-containing diets, urine and feces were collected on day 5 of the treatment. Urine samples were diluted with 4

volumes of 50% acetonitrile and centrifuged at 18,000 *g* for 10 minutes, and the supernatants were subjected to the analysis. Fecal samples were completely dried at room temperature and minced by mortar and pestle, then 100 mg of samples were extracted with 1 ml of 50% acetonitrile at room temperature for 2 hours under continuous vortexing. Fecal extracts were diluted with the same volume of 50% acetonitrile before being loaded into the UPLC-TOFMS system (Waters). I3C standard was dissolved in DMSO and diluted in 50% acetonitrile to the final concentration of 0.001%–0.1%. 4′-OH and N^2-OH PhIP standards were dissolved in 50% acetonitrile to a final concentration of 20–500 nM. An ACQUITY UPLC BEH C_{18} column (Waters) was used to separate samples at 30°C. The mobile phase flow rate was 0.5 ml/min, with a gradient ranging from water to 95% aqueous acetonitrile containing 0.1% formic acid over a 10-minute run. The Q-ToF Premier Mass Spectrometer (Waters) was operated in the positive electrospray ionization (ESI) mode. Capillary voltage and cone voltage were maintained at 3 kV and 20 V, respectively. Source temperature and desolvation temperatures were set at 120°C and 350°C, respectively. Nitrogen was used as both cone gas (50 l/h) and desolvation gas (600 l/h) and argon as collision gas. For accurate mass measurement, the TOFMS was calibrated with sodium formate solution (range *m/z* 100–1,000) and monitored by the intermittent injection of the lock mass sulfadimethoxine ($[M + H]^+$ = 311.0814 *m/z*) in real time. MS/MS fragmentation was conducted with collision energy ramping from 15 to 35 eV.

Data processing and PLS-DA. Chromatographic and spectral data were first centroided and integrated and then deconvoluted by MarkerLynx software (Waters) to generate a multivariate data matrix. For the purpose of the global metabolite analysis, the relative intensity of each ion was calculated as the percentage of total ion counts in the whole chromatogram. The entire data set was further exported into SIMCA-P+ 11 software (Umetrics) and transformed by mean-centering and Pareto scaling, a technique that increases the importance of low-abundance ions without significant amplification of noise. PLS-DAs were carried out to represent the major latent variables in the data matrix and were described in a scores scatter plot. Three components (axes) were assigned to build up each model and were fit for the grouping/separation of the samples (35). After identification of the contributing ions for each group, chromatograms were individually constructed with the *m/z* value of the each identified ion, with an allowance of 50-ppm *m/z* deviations, to measure the actual intensities. The abundance of each ion was determined from the integrated peak area in the constructed chromatogram, in which the *y* axis represents ion count per second.

In vitro metabolism of PhIP. Lungs from 2- to 3-month-old normal chow– or I3C-fed mice were homogenized, and microsomes were prepared as described previously (51). Microsomal incubations were carried out in 20 mM PBS, pH 7.4, containing 1 mg/ml microsomal protein, 2 mM $MgCl_2$, 20 μM PhIP, and 1 mg/ml freshly prepared β-NADPH in a final volume of 100 μl. After 20 minutes of incubation at 37°C, the reaction mix was mixed with equal volumes of acetonitrile, centrifuged at 18,000 *g* for 10 minutes, and the supernatants were subjected to UPLC-TOFMS analysis with ESI^+ mode. Corresponding peaks for 4′-OH PhIP and N^2-OH PhIP were identified from comparison of chromatographs and retention times with those of the 4′-OH and N^2-OH PhIP standards analyzed under the same conditions. Peak areas for hydroxylated PhIP were calculated from the chromatographs constructed with *m/z* = 241.1089 (50-ppm *m/z* deviations). The actual amounts of hydroxylated PhIP products were determined from the comparison of integrated peak areas with those of 4′-OH and N^2-OH PhIP standards run at various concentrations under the same conditions. Microsomal PhIP hydroxylase activity was calculated from the amount of hydroxylated PhIP generated by 1 μg of microsomal protein within 1 minute (pmol/min/μg).

Statistics. All data were analyzed by 2-tailed and unpaired Student's *t* test or Mann-Whitney *U* test for the significant difference between the mean values using Statcel (OMS Publishing Inc.) for Macintosh. Significant differences determined by Mann-Whitney *U* test are marked with dagger symbols. A *P* value of less than 0.05 was considered significant.

Acknowledgments

We thank Linda Byrd, Xiaochao Ma, Yueying Zhen, and Kristopher Krausz for technical advice; Vasilis Vasiliou and Jeffrey Idle for helpful comments; and Shuhei Tomita for providing Southern blot probes for Arnt and Hif-1α. Shinji Ito was supported in part by a fellowship from the Japanese Society for the Promotion of Science (JSPS). This study was supported by the National Cancer Institute Intramural Research Program.

Received for publication January 29, 2007, and accepted in revised form April 24, 2007.

Address correspondence to: Frank J. Gonzalez, Laboratory of Metabolism, National Cancer Institute, Building 37, Room 3106, Bethesda, Maryland 20892, USA. Phone: (301) 496-9067; Fax: (301) 496-8419; E-mail: fjgonz@helix.nih.gov.

1. Brooks, R.A., Gooderham, N.J., Edwards, R.J., Boobis, A.R., and Winton, D.J. 1999. The mutagenicity of benzo[a]pyrene in mouse small intestine. *Carcinogenesis.* **20**:109–114.
2. Kaminsky, L.S., and Zhang, Q.Y. 2003. The small intestine as a xenobiotic-metabolizing organ. *Drug Metab. Dispos.* **31**:1520–1525.
3. Lindell, M., Lang, M., and Lennernas, H. 2003. Expression of genes encoding for drug metabolising cytochrome P450 enzymes and P-glycoprotein in the rat small intestine; comparison to the liver. *Eur. J. Drug Metab. Pharmacokinet.* **28**:41–48.
4. Zhang, Q.Y., Dunbar, D., and Kaminsky, L.S. 2003. Characterization of mouse small intestinal cytochrome P450 expression. *Drug Metab. Dispos.* **31**:1346–1351.
5. Ma, Q. 2001. Induction of CYP1A1. The AhR/DRE paradigm: transcription, receptor regulation, and expanding biological roles. *Curr. Drug Metab.* **2**:149–164.
6. Whitlock, J.P., Jr. 1999. Induction of cytochrome P4501A1. *Annu. Rev. Pharmacol. Toxicol.* **39**:103–125.
7. Uno, S., et al. 2004. Oral exposure to benzo[a]pyrene in the mouse: detoxication by inducible cytochrome P450 is more important than metabolic activation. *Mol. Pharmacol.* **65**:1225–1237.
8. Choudhary, D., Jansson, I., Schenkman, J.B., Sarfarazi, M., and Stoilov, I. 2003. Comparative expression profiling of 40 mouse cytochrome P450 genes in embryonic and adult tissues. *Arch. Biochem. Biophys.* **414**:91–100.
9. Nebert, D.W., and Dalton, T.P. 2006. The role of cytochrome P450 enzymes in endogenous signalling pathways and environmental carcinogenesis. *Nat. Rev. Cancer.* **6**:947–960.
10. Lanza, D.L., and Yost, G.S. 2001. Selective dehydrogenation/oxygenation of 3-methylindole by cytochrome p450 enzymes. *Drug Metab. Dispos.* **29**:950–953.
11. Semenza, G.L. 2006. Regulation of physiological responses to continuous and intermittent hypoxia by hypoxia-inducible factor 1. *Exp. Physiol.* **91**:803–806.
12. Kaelin, W.G. 2005. Proline hydroxylation and gene expression. *Annu. Rev. Biochem.* **74**:115–128.
13. Tomita, S., Sinal, C.J., Yim, S.H., and Gonzalez, F.J. 2000. Conditional disruption of the aryl hydrocarbon receptor nuclear translocator (Arnt) gene leads to loss of target gene induction by the aryl hydrocarbon receptor and hypoxia-inducible factor 1alpha. *Mol. Endocrinol.* **14**:1674–1681.
14. Madison, B.B., et al. 2002. Cis elements of the villin gene control expression in restricted domains of the vertical (crypt) and horizontal (duodenum, cecum) axes of the intestine. *J. Biol. Chem.* **277**:33275–33283.
15. el Marjou, F., et al. 2004. Tissue-specific and inducible Cre-mediated recombination in the gut epithelium. *Genesis.* **39**:186–193.
16. Pringault, E., Arpin, M., Garcia, A., Finidori, J., and Louvard, D. 1986. A human villin cDNA clone to investigate the differentiation of intestinal and kidney cells in vivo and in culture. *EMBO J.* **5**:3119–3124.
17. Stresser, D.M., Bailey, G.S., and Williams, D.E. 1994. Indole-3-carbinol and beta-naphthoflavone induction of aflatoxin B1 metabolism and cytochromes P-450 associated with bioactivation and detoxication of aflatoxin B1 in the rat. *Drug Metab. Dispos.* **22**:383–391.
18. Tomita, S., et al. 2003. Defective brain development

in mice lacking the Hif-1alpha gene in neural cells. *Mol. Cell. Biol.* **23**:6739–6749.
19. Semenza, G.L. 1999. Regulation of mammalian O2 homeostasis by hypoxia-inducible factor 1. *Annu. Rev. Cell Dev. Biol.* **15**:551–578.
20. Scharte, M., Han, X., Bertges, D.J., Fink, M.P., and Delude, R.L. 2003. Cytokines induce HIF-1 DNA binding and the expression of HIF-1-dependent genes in cultured rat enterocytes. *Am. J. Physiol. Gastrointest. Liver Physiol.* **284**:G373–G384.
21. Karhausen, J., et al. 2004. Epithelial hypoxia-inducible factor-1 is protective in murine experimental colitis. *J. Clin. Invest.* **114**:1098–1106. doi:10.1172/JCI200421086.
22. Pescador, N., et al. 2005. Identification of a functional hypoxia-responsive element that regulates the expression of the egl nine homologue 3 (egln3/phd3) gene. *Biochem. J.* **390**:189–197.
23. Tijet, N., et al. 2006. Aryl hydrocarbon receptor regulates distinct dioxin-dependent and dioxin-independent gene batteries. *Mol. Pharmacol.* **69**:140–153.
24. Ma, X., et al. 2007. Mouse lung CYP1A1 catalyzes the metabolic activation of 2-amino-1-methyl-6-phenylimidazo[4,5-b]pyridine (PhIP). *Carcinogenesis.* **28**:732–737.
25. Choudhary, D., Jansson, I., Stoilov, I., Sarfarazi, M., and Schenkman, J.B. 2005. Expression patterns of mouse and human CYP orthologs (families 1–4) during development and in different adult tissues. *Arch. Biochem. Biophys.* **436**:50–61.
26. Poland, A., and Glover, E. 1990. Characterization and strain distribution pattern of the murine Ah receptor specified by the Ahd and Ahb-3 alleles. *Mol. Pharmacol.* **38**:306–312.
27. Poland, A., Palen, D., and Glover, E. 1994. Analysis of the four alleles of the murine aryl hydrocarbon receptor. *Mol. Pharmacol.* **46**:915–921.
28. Ema, M., et al. 1994. Dioxin binding activities of polymorphic forms of mouse and human arylhydrocarbon receptors. *J. Biol. Chem.* **269**:27337–27343.
29. Nebert, D.W., Dalton, T.P., Okey, A.B., and Gonzalez, F.J. 2004. Role of aryl hydrocarbon receptor-mediated induction of the CYP1 enzymes in environmental toxicity and cancer. *J. Biol. Chem.* **279**:23847–23850.
30. Middleton, E., Jr., Kandaswami, C., and Theoharides, T.C. 2000. The effects of plant flavonoids on mammalian cells: implications for inflammation, heart disease, and cancer. *Pharmacol. Rev.* **52**:673–751.
31. Wattenberg, L.W. 1975. Effects of dietary constituents on the metabolism of chemical carcinogens. *Cancer Res.* **35**:3326–3331.
32. Auborn, K.J., et al. 2003. Indole-3-carbinol is a negative regulator of estrogen. *J. Nutr.* **133**(7 Suppl.):2470S–2475S.
33. Aggarwal, B.B., and Ichikawa, H. 2005. Molecular targets and anticancer potential of indole-3-carbinol and its derivatives. *Cell Cycle.* **4**:1201–1215.
34. Bjeldanes, L.F., Kim, J.Y., Grose, K.R., Bartholomew, J.C., and Bradfield, C.A. 1991. Aromatic hydrocarbon responsiveness-receptor agonists generated from indole-3-carbinol in vitro and in vivo: comparisons with 2,3,7,8-tetrachlorodibenzo-p-dioxin. *Proc. Natl. Acad. Sci. U. S. A.* **88**:9543–9547.
35. Eriksson, L., et al. 2006. *Multi- and megavariate data analysis part I: basic principles and applications*. Umetrics Academy. Umeå, Sweden. 425 pp.
36. Grose, K.R., and Bjeldanes, L.F. 1992. Oligomerization of indole-3-carbinol in aqueous acid. *Chem. Res. Toxicol.* **5**:188–193.
37. Uno, S., et al. 2006. Oral benzo[a]pyrene in Cyp1 knockout mouse lines: CYP1A1 important in detoxication, CYP1B1 metabolism required for immune damage independent of total-body burden and clearance rate. *Mol. Pharmacol.* **69**:1103–1114.
38. Delescluse, C., Lemaire, G., de Sousa, G., and Rahmani, R. 2000. Is CYP1A1 induction always related to AHR signaling pathway? *Toxicology.* **153**:73–82.
39. Shertzer, H.G. et al. 2007. 7H-dibenzo[c,g]carbazole metabolism by the mouse and human CYP1 family of enzymes. *Carcinogenesis.* In press.
40. Girardi, M., et al. 2001. Regulation of cutaneous malignancy by gammadelta T cells. *Science.* **294**:605–609.
41. Rose-Hellekant, T.A., Gilchrist, K., and Sandgren, E.P. 2002. Strain background alters mammary gland lesion phenotype in transforming growth factor-alpha transgenic mice. *Am. J. Pathol.* **161**:1439–1447.
42. Wang, Y., et al. 2004. A chemically induced model for squamous cell carcinoma of the lung in mice: histopathology and strain susceptibility. *Cancer Res.* **64**:1647–1654.
43. Woodworth, C.D., et al. 2004. Strain-dependent differences in malignant conversion of mouse skin tumors is an inherent property of the epidermal keratinocyte. *Carcinogenesis.* **25**:1771–1778.
44. Mimura, J., et al. 1997. Loss of teratogenic response to 2,3,7,8-tetrachlorodibenzo-p-dioxin (TCDD) in mice lacking the Ah (dioxin) receptor. *Genes Cells.* **2**:645–654.
45. Barbieri, O., Ognio, E., Rossi, O., Astigiano, S., and Rossi, L. 1986. Embryotoxicity of benzo(a)pyrene and some of its synthetic derivatives in Swiss mice. *Cancer Res.* **46**:94–98.
46. Yu, Z., et al. 2006. Indole-3-carbinol in the maternal diet provides chemoprotection for the fetus against transplacental carcinogenesis by the polycyclic aromatic hydrocarbon, dibenzo[a,l]pyrene. *Carcinogenesis.* **27**:2116–2123.
47. Niwa, T., et al. 2001. Metabolism and interaction of bisphenol A in human hepatic cytochrome P450 and steroidogenic CYP17. *Biol. Pharm. Bull.* **24**:1064–1067.
48. Maffini, M.V., Rubin, B.S., Sonnenschein, C., and Soto, A.M. 2006. Endocrine disruptors and reproductive health: the case of bisphenol-A. *Mol. Cell. Endocrinol.* **254–255**:179–186.
49. Williamson, M.A., Gasiewicz, T.A., and Opanashuk, L.A. 2005. Aryl hydrocarbon receptor expression and activity in cerebellar granule neuroblasts: implications for development and dioxin neurotoxicity. *Toxicol. Sci.* **83**:340–348.
50. Dobbin, K.K., Kawasaki, E.S., Petersen, D.W., and Simon, R.M. 2005. Characterizing dye bias in microarray experiments. *Bioinformatics.* **21**:2430–2437.
51. Yu, A.M., Idle, J.R., Krausz, K.W., Kupfer, A., and Gonzalez, F.J. 2003. Contribution of individual cytochrome P450 isozymes to the O-demethylation of the psychotropic beta-carboline alkaloids harmaline and harmine. *J. Pharmacol. Exp. Ther.* **305**:315–322.